# A Multi-Layered Approach for Detecting Alzheimer's Disease (AD) Using Deep Learning Model

Nutalapati Ashok[1*], Dr. K. Gangadhara Rao[2]

*[1]Research Scholar, Department of CSE, Acharya Nagarjuna University, nutalapati.ashok@gmail.com*

*[2]Principal, University College of Science, Acharya Nagarjuna University, HOD, Department of CSE, Acharya Nagarjuna University*

***Corresponding Author:** Nutalapati Ashok*

**Research Scholar, Department of CSE, Acharya Nagarjuna University, nutalapati.ashok@gmail.com*

**Abstract:** Alzheimer's disease (AD) is a chronic brain disorder that affects the brain cells finally. The common cause of AD is dementia which reduces memory, thinking, behavior, and social skills. All these changes affect a person's ability to function. It is challenging to detect the disease in the early stages. Some of the most common diagnosing techniques are Magnetic Resonance Imaging (MRI), Positron Emission Tomography (PET), and Single Photon Emission Computed Tomography (SPECT). These techniques provide information regarding the external and internal regions of the brain activities for diagnosing AD. Sometimes with the above methods, it is impossible to analyze AD accurately. The retina is a significant part of the eye which provides the vision to humans. Several studies made that the retina reveals that AD patients have some variations in the retina layers in addition to brain changes. Therefore, the retina becomes a biomarker for diagnosing AD. There are different techniques available for an eye examination. Most noticeable are Fundus Imaging and Optical Coherence Tomography (OCT). This paper introduces multi-layered Deep Learning (MLDL) to diagnose AD in the early stages from retinal abnormalities. Results show that the proposed approach achieved 98.7% accuracy in detecting AD.

**Keywords:** Magnetic Resonance Imaging (MRI), Positron Emission Tomography (PET), and Single Photon Emission Computed Tomography (SPECT).

## 1. INTRODUCTION

Alzheimer’s disease (AD), the most common form of dementia, is a major public health and clinical challenge globally [1]. Despite decades in research, the pathophysiology of AD remains unclear. The current thinking is that the neuropathology of AD, as characterized by accumulation of misfolded amyloid-β and tau protein, begins years before the onset of clinical symptoms. Given this long natural history, there are opportunities for early disease detection and thus timely intervention [2] [3]. Indeed, recent clinical trials have suggested the efficacy of certain measures (eg, lifestyle interventions or medication) in improving symptoms or slowing progression of AD [4]. OCT and OCTA generate large-scale, high-dimensional and multimodal retinal scans, which require tedious and time-consuming readings to be performed by experts. As in similar medical diagnostic fields, machine or deep learning-based automated approaches can significantly enhance physicians’ ability to efficiently diagnose abnormalities in the retina.

Optical coherence tomography (OCT) is a recently established imaging technique to describe different information about the internal structures of an object and to image various aspects of biological tissues, such as structural information, blood flow, elastic parameters, change of polarization states, and molecular content.[5] In contrast to OCT technology development which has been a field of active research since 1991, OCT image segmentation has only been more fully explored during the last decade. Segmentation, however, remains one of the most difficult and at the same time most commonly required steps in OCT image analysis. No typical segmentation method exists that can be expected to work equally well for all tasks. [6]

It should be noted that OCT is not the only possible device for assessing retinal pathologies; the field of ophthalmology was revolutionized in 1851 with the invention of the ophthalmoscope by Hermann von Helmholtz [7] as for the first time detailed examinations of the interior of the eye could be made in living patients. Fundus photography (a low powered microscope attached with a camera),[8] fluorescein Angiography [5] (photographing the retina by injecting fluorescent dyes) and Retinal thickness analyzer (RTA)[9] are other modalities proposed for

diagnosis of retinal malfunctions. The latter is capable of rapidly obtaining retinal thickness map covering an area of 3 × 3 mm. The oblique projection of a narrow laser slit beam on retina and recording the backscattered light are the principles of this method.[10] Furthermore, confocal scanning laser ophthalmoscopy (CSLO)[11] provides a three-dimensional topographic representationof the optic disk and peripapillary retina, which is constructed from a series of two-dimensional slices. This three-dimensional representation consists of 256 × 256 (65,536) pixel elements, each of which is a measurement of retinal height at its corresponding location. Three topography images are usually acquired in a single session and thereafter are automatically aligned and averaged to obtain a single mean topography image. Although the CSLO is similar, in many respects, to a CT scan, the light rays used for CSLO cannot penetrate tissue; this limits this modality to depicting the surface topography of the optic disk and para-papillary retina. [12]

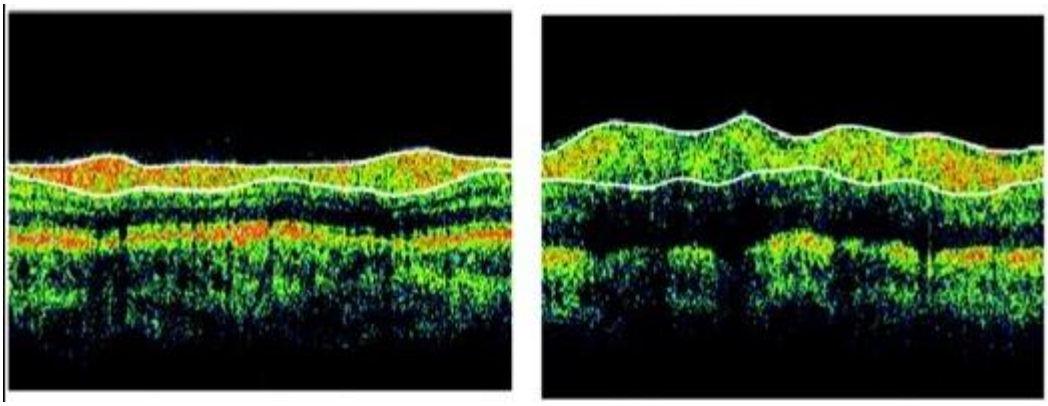

**Figure 1** (a) Normal OCT Images and 1(b) Ad affected OCT Image

## LITERATURE SURVEY

Mayer[13] calculated the RNFL thickness in circular SDOCT B-scans from 5 normal and 7 glaucoma eyes using Fuzzy C-means clustering technique without the need of parameter adaptation for pathological data. They reported that 97% of the upper and 74% of the lower RNFL layer boundary points lied within a two pixel range from the manual segmentation of the evaluation data set.

Baroni[14] used edge likelihood function maximizing for boundary detection. Along the A-scans, median filtering was applied (as 1D filter of 5 pixels); this eliminated isolated noisy pixels without losing small details. In the second step, the reflectivity values were summed row by row, to obtain a longitudinal cumulative grey level histogram. Bagci[15] in 2007 used correlation of axial A-scans to find six retinal layers and many papers used the same method for retinal thickness analysis in OCT datasets.

Recently in 2010, Mayer[16] used the minimization of an energy function consisting of gradient and local smoothing terms on 72 scans from glaucoma patients and 132 scans from normal subjects. A mean absolute error per A-Scan of 2.9 μm was achieved on glaucomatous eyes, and 3.6 μm on healthy eyes which proved that the approach provided a reliable tool for extracting diagnostic relevant parameters from OCT B-Scans for glaucoma diagnosis.

In 2011, Ghorbel[17] proposed a method for the segmentation of eight retinal layers in Heidelberg spectralis SDOCT images. The approach was based on global segmentation algorithms, such as active contours and Markov random fields. Moreover, a Kalman filter was designed to model the approximate parallelism between the photoreceptor segments and to detect them. The performance of the algorithm was tested on a set of 700 retinal images acquired in-vivo from healthy subjects.

Vermeer[18] in 2011 presented a method for three-dimensional retinal layer segmentation in OCT images by a flexible method that learned from provided examples. Parts of representative OCT scans were manually segmented and used by the algorithms to learn from. Learning and classification of pixels was done by a support vector machine.

Smoothness of the detected interfaces was guaranteed by the level set regularization that was applied after the pixel classification. The procedure was the same for all layers, except for the manually segmented data used to train the classifier. RMS errors for the top and bottom of the retina were between 4 and 6 μm, while the errors for intra-retinal interfaces were between 6 and 15 μm.

### 2.1. Image Acquisition and Preprocessing

Image acquisition is done by OCT camera which is shown in figure 2; it is a kind of imaging technique used to examine the different eye related disease. During the OCT process, six linear scans centered on the Optical Nerve Head (ONH) is obtained, and the OCT software derives the ONH parameters in an automatic manner. The scan also gives horizontal and vertical cup-to-disc ratios. For the measurement of Retinal Nerve Fibre Layer (RNFL), the usable RNFL thickness circle scan mode which consists of 3 scans that are circular with twice the radius of 3.4 mm centered on the ONH should be used. Thus the overall, average and quadrant RNFL thicknesses should be calculated automatically. The images obtained from OCT device can saved as bitmap file with extension .bmp. The size of each image obtained is 523 kilobytes and the dimension of each image is 560 X 319.

**Fig 2:** OCT device and OCT image obtained on the screen

After image acquisition is over, preprocessing is performed by using median filter which removes unwanted noises from OCT images.

### 2.2. Segmentation Using Wavelet Networks

For the different steps involved in OCT image classification, segmentation is the most important stage of all. Image segmentation can be defined as the method of separation of an original image into multiple segments. Segmentation using wavelet network (WN) is a promising approach in medical imaging. In this method a family of wavelet scan is formed from a function, called "mother wavelet," that can be confined in a finite interval. After mother wavelet is obtained, "daughter wavelets" are then formed by shifting and scaling of mother wavelet. Wavelets are mainly useful for compressing image data from a larger one [19-22]. A three-layer FGWN with one hidden layer is employed in OCT image segmentation is discussed here. The procedure for image segmentation in this paper is as follows. The first step is to normalize the input data using RGB normalization. Due to the desirable features of Mexican Hat wavelet such as effective calculation, Gaussian structure adaptability and robustness against noise for creating mother wavelets [25]. After that daughter wavelets are formed, thus producing a wavelet lattice. Wavelet lattice can be defined as a hyper shape of shift and scale values of wavelets. The hyper shape has huge dimensions that should be decreased and after that necessary wavelets should be selected. All of these are accomplished through two stages of screening.

The structure of wavelet network output signal with one output f, an array of X inputs and q wavelons in the hidden layer is given by the eq. 1.

$$\sum_{i=1}^{n} w_i \psi_{pi,qi}(X) = \sum_{i=1}^{n} w_i 2^{-p_i d/2} \psi(2^{pi} X - qi) \qquad (1)$$

where wi, i =1,2,...,n ,are weight coefficients ,ψpi ,qi are dilated and translated versions of a mother wavelet function, ψ and pi, qi are scale and shift parameters, respectively [24]. In FGWN, after determining the structure, the weights wi in (1) can be obtained through linear estimation techniques. In this study, a constructive method is employed to build an FGWN. The FGWN structure is determined by the following algorithm. This first stage is considered as the preprocessing stage in which the input data are normalized to a certain range in order to avoid data scattering. Here the values of R, G, and B matrices of each color OCT image are mapped into [0, 1] range by performing normalization process [26]. Next stage is to select the mother wavelet using Mexican hat wavelet [27]. It is expressed as in eq.2.

$$\psi(x) = \eta\|x\| = (d - \|x\|\hat{}2)e\hat{}(-\|x\|\hat{}2|2) \qquad (2)$$

The next stage is to select the minimum and maximum scale levels in the form $P_{min}$ $P_{max}$ pp and shift parameters. After that the wavelet lattice is employed with the help of eq.3.

$$\psi_{pi.qj}(x) = 2^{-p_i d/2} \psi(2^{p_i} x - q_j) \qquad (3)$$

Next is to employ two stages of screening, primary and secondary. In the former stage, for every scale level selected Ik set is formed for each input vector. In the later stage, the shift and scale parameters of wavelets that are selected in at least two set of the sets in the former stage and set I is formed. After the above stage is completed, next is to form the wavelet matrix as in eq.4.

$$W = \begin{bmatrix} \psi_1(x^{(1)}) \ldots\ldots \psi_M(x^{(1)}) \\ \psi_1(x^{(2)}) \ldots\ldots \psi_M(x^{(2)}) \\ \ldots\ldots\ldots\ldots\ldots\ldots \\ \psi_1(x^{(P)}) \ldots\ldots \psi_M(x^{(P)}) \end{bmatrix} \qquad (4)$$

After the formation of the wavelet matrix, an efficient model structure has been implemented using the orthogonal least squares (OLS) algorithm. The algorithm is as follows: At first, the most necessary wavelets in W are selected and then the non selected wavelets are made orthogonal to the selected one. In the second step, the remaining necessary wavelets are again selected and non selected wavelets are made orthogonal to the selected one. Therefore the wavelet that is selected secondly with addition to the first one can be used for the best approximation. The above step is repeated for the remaining wavelets. [28]. After employing this stage, wavelet network is constructed by selecting the number of wavelons and its weight is calculated using least squares method. The segmentation process is illustrated in figure 3.

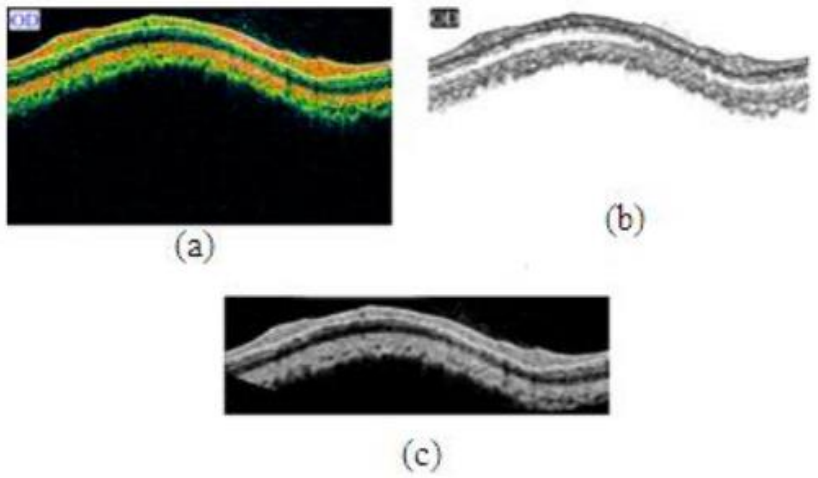


**Fig.3.** Segmentation process (a) Original image (b) Mexican hat feature output (c) Segmented Image

### 2.3. Feature Extraction and Selection

Feature extraction is the process of extracting the necessary features of OCT images for the early diagnosis of AD. In this research we have extracted different features such as ellipticity, ratio between thickness, curvature variance, salience variance, red texture, perimeter, area, moments, histogram, entropy calculation, Gabor, gradient and SURF. From the extracted features next is to select the required features using wrapper model. This model includes a criterion for feature evaluation, a strategy for searching and a criterion for stopping. This model makes use of the learning algorithm as the criterion for evaluation. This makes sure that the feature selected is matched to the algorithm used for machine learning. Wrappers are very expensive in computation as it requires the machine learning algorithm to be executed in each and every iteration, can be used for datasets having low dimensional values. Search strategies have the property to generate various feature combinations to traverse through the feature space. The criterion used for stopping is to stop generating and evaluating new feature subsets while adding or removing features which is not making any improvements in the performance [29]. For N features there exist 2N potential subsets. The feature search therefore plays a most significant part in wrappers. The different search techniques included in wrapper model are exponential, sequential and randomized searches.

### 2.4. Classification using Radial Basis Function

The RBF network performs function mapping that are similar with the multi-layer neural network, but its structure and function are not similar. A RBF can be called as a local network which uses supervised training. The RBF classifier is having the input layer with a set of n units that can receive the n -dimensional input feature vector elements. The n elements having input vector x are given to the input of l hidden functions. The output from the hidden function is multiplied by the weighting factor w(i, j), which is given as input to the output layer of the network y(x). Therefore for each RBF unit k, k = 1, 2,3,..., l the center is selected as the mean value of the sample patterns belong to class k as in eq. 5.

$$\square_k = \frac{1}{N_k}\sum_{i=1}^{N_k} x_k^i$$

where ♢ is the eigenvector of the ith image in the class k, and Nk is the total number of trained images in class k. As the RBF neural network is type of neural networks, the hidden layer activation function is determined by input vector and prototype vector distance. We have compared the above techniques for the OCT images and found that RBF produces better results than BP. Also RBF requires less time than BP during execution.

## 3. EXPERIMENTAL RESULTS

The experiments are conducted by using python programming language with 8 GB RAM and 128 SDD hard drive to process the large datasets.

### 3.1. Performance Metrics

The confusion matrix is used to analyze the classification algorithm performance. Measuring the performance with a confusion matrix gives a better for find the accurate errors. It is also used to solve several classification issues. This can be applied for classification of binary issues and also for multiclass classification issues. The count values are based on various attributes such as

**TP:** In this the actual value of true (disease present) and predicted value is true (disease present).

**TN:** The actual value is true (disease present) and predicted value is false (No disease).

**FP:** The actual value is false (No disease) and predicted value is true (disease present).

**FN:** The actual value is false (No disease) and predicted value is false (No disease).

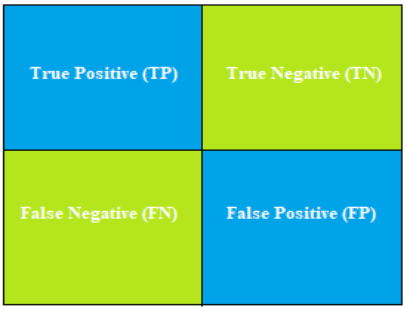


**Figure 3:** Confusion Matrix

**Sensitivity ($S_n$):** Sensitivity, recall, or the TP rate (TPR) is the fraction of positive values out of the total actual positive instances (i.e., the proportion of actual positive cases that are correctly identified):

$$S_n = \frac{TP}{TP + FN}$$

**Specificity ($S_p$):** Specificity gives the fraction of negative values out of the total actual negative instances. In other words, it is the proportion of actual negative cases that are correctly identified. The FP rate is given by (1 – specificity):

$$S_p = \frac{TN}{TN + FP}$$

**Precision (P):** Precision or the positive predictive value, is the fraction of positive values out of the total predicted positive instances. In other words, precision is the proportion of positive values that were correctly identified:

$$P = \frac{TP}{TP+FP}s$$

**Accuracy (Acc):** Accuracy shows the total number of prediction that is correct. Actual and predicted values are correct. It is represented with below formula.

$$Acc = \frac{TP + TN}{TP + FP + TN + FN}$$

**F1-Score (F1S):** The F1-score combines the precision and recall of a classifier into a single metric by taking their harmonic mean.

$$F1S = 2 * \frac{P * S_n}{P + S_n}$$

**Table 2 Shows the Performance of Existing and Proposed Algorithms for detection of AD from OCT Images dataset**

| | RF | CNN | MLDL |
|---|---|---|---|
| **Sensitivity (SE)** | 77.22 | 86.76 | 98.98 |
| **Specificity (SP)** | 81.54 | 85.76 | 98.56 |
| **Precision (PE)** | 80.65 | 85.43 | 98.34 |
| **Accuracy (ACC)** | 81.66 | 87.52 | 97.76 |
| **F1-Score** | 82.12 | 87.53 | 97.58 |

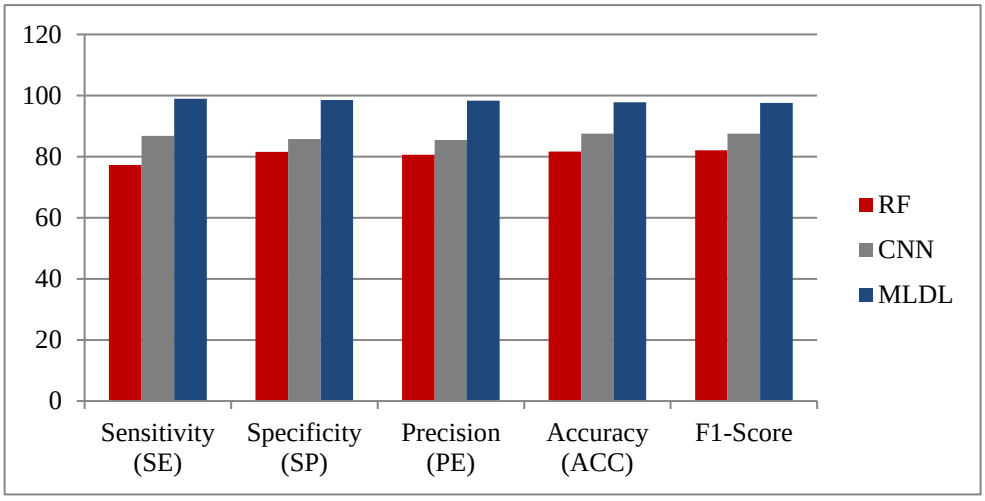


**Table 2** Shows the Performance of Existing and Proposed Algorithms for detection of Normal Samples from AD

| | RF | CNN | MLDL |
|---|---|---|---|
| **Sensitivity (SE)** | 77.22 | 86.76 | 98.98 |
| **Specificity (SP)** | 81.54 | 85.76 | 98.56 |
| **Precision (PE)** | 80.65 | 85.43 | 98.34 |
| **Accuracy (ACC)** | 81.66 | 87.52 | 97.76 |
| **F1-Score** | 82.12 | 87.53 | 97.58 |

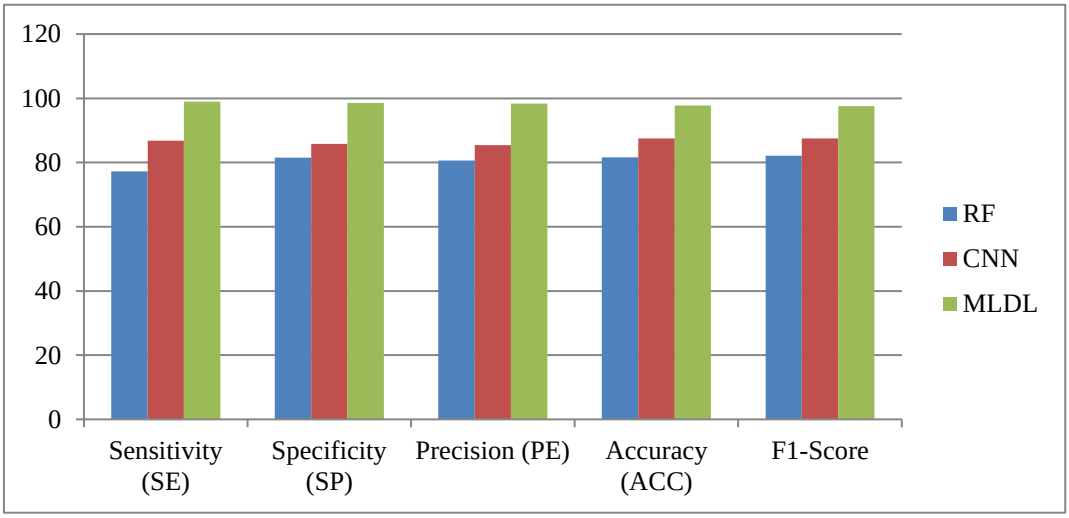


## CONCLUSION

In this paper, the multi-layered Deep Learning (MLDL) is implemented by utilizing the OCT retinal images. The proposed system mainly focused on detecting and diagnosing the AD from the OCT images. Here we have selected the OCT images which are affected with AD. AD is a prolonged progressive disease. Therefore, detection of the

disease in its early stages is vital. From the medical literature it is revealed that the most recent findings about AD-related changes in the retina, which are observable through OCT examination. The proposed approach focuses on layer thickness changes in particular retinal layers such as Retinal Nerve Fiber, Ganglion Cell, and Inner-Plexiform Layers. Usually, the OCT scan is segmented automatically (sometimes with manual interventions) to identify these layers; and then layer average thickness values are computed.

## REFERENCES


[1] Alzheimer's Association. 2016 Alzheimer's disease facts and figures. Alzheimers Dement 2016;12:459–509.
[2] Jack CR, Knopman DS, Jagust WJ, et al. Tracking pathophysiological processes in Alzheimer's disease: an updated hypothetical model of dynamic biomarkers. Lancet Neurol 2013;12:207–16.
[3] Sperling R, Mormino E, Johnson K. The evolution of preclinical Alzheimer's disease: implications for prevention trials. Neuron 2014;84:608–22.
[4] Cummings J, Passmore P, McGuinness B, et al. Souvenaid in the management of mild cognitive impairment: an expert consensus opinion. Alzheimers Res Ther 2019;11:73.
[5] Huang D, Swanson EA, Lin CP, Schuman JS, Stinson WG, Chang W, et al. Optical coherence tomography. Science. 1991;254:1178–81.
[6] DeBuc DC. A Review of Algorithms for Segmentation of Retinal Image Data Using Optical Coherence Tomography. Image Segmentation In Tech.
[7] von Helmholtz H. World Encyclopedia. New York: Oxford University Press; 1851. Optalmoscope.
[8] Delori FC, Gragoudas ES. Monochromatic ophthalmoscopy and fundus photography. The normal fundus. Arch Ophthalmol. 1977;95:861–8.
[9] Novotny HR, Alvis DL. A method of photographing fluorescence in circulating blood in the human retina. Circulation. 1961;24:82–6.
[10] Zeimer R, Shahidi M. A new method for rapid mapping of the retinal thickness at the posterior pole. Invest Ophthalmol Vis Sci. 1996;37:1994–2001.
[11] Rohrschneider K, Burk RO, Kruse FE, Volcker HE. Reproducibility of the optic nerve head topography with a new laser tomographic scanning device. Ophthalmology. 1994;101:1044–9.
[12] Blumenthal EZ, Weinreb RN. Assessment of the retinal nerve fiber layer in clinical trials of glaucoma neuroprotection. Surv Ophthalmol. 2001;45(Suppl 3):S305–12.
[13] Mayer MA, Tornow RP, Bock R, Hornegger J, Kruse FE. Automatic nerve fiber layer segmentation and geometry correction on spectral domain OCT Images using fuzzy c-means clustering. The Association for Research in Vision and Ophthalmology, Inc. (ARVO) (Annual Meeting) in Fort Lauderdale, Florida, USA. 2008.
[14] Baroni M, Fortunato JG, Torre AL. Towards quantitative analysis of retinal features in optical coherence tomography. Med Eng Phys. 2007;29:432–41.
[15] Bagci AM, Shahidi M, Ansari R, Blair M, Blair NP, Zelkha R. Thickness profile of retinal layers by opticalcoherence tomography image segmentation. Am J Ophthalmol. 2008;146:679–87.
[16] Mayer MA, Hornegger J, Mardin CY, Tornow RP. Retinal nerve fiber layer segmentation on FD-OCT scans of normal subjects and glaucoma patients. Biomed Opt Express. 2010;1:1358–83.
[17] Ghorbel I, Rossant F, Bloc I, Tic S, Paques M. Automated segmentationof macular layers in OCT images and quantitative evaluation of performances. Pattern Recognit. 2011;44:1590–603.
[18] Vermeer KA, van der Schoot J, Lemij HG, de Boer JF. Automated segmentation by pixel classification of retinal layers in ophthalmic OCT images. Biomedical Opt Express. 2011;2:1743–56.


DOI: https://doi.org/10.15379/ijmst.v10i3.3528